BIOCHEMISTRY
including biophysical chemistry & molecular biology

Article

pubs.acs.org/biochemistry

Shewanella oneidensis Cytochrome *c* Nitrite Reductase (ccNiR) Does Not Disproportionate Hydroxylamine to Ammonia and Nitrite, Despite a Strongly Favorable Driving Force

Matthew Youngblut,[†,∥] Daniel J. Pauly,[†] Natalia Stein,[†] Daniel Walters,[†,⊥] John A. Conrad,[†,‡] Graham R. Moran,[†] Brian Bennett,[§] and A. Andrew Pacheco*[,†]

[†]Department of Chemistry and Biochemistry, University of Wisconsin—Milwaukee, Milwaukee, Wisconsin 53211, United States

[‡]Department of Chemistry, University of Nebraska—Omaha, Omaha, Nebraska 68182, United States

[§]Department of Biophysics, Medical College of Wisconsin, Milwaukee, Wisconsin 53226, United States

Supporting Information

ABSTRACT: Cytochrome *c* nitrite reductase (ccNiR) from *Shewanella oneidensis*, which catalyzes the six-electron reduction of nitrite to ammonia *in vivo*, was shown to oxidize hydroxylamine in the presence of large quantities of this substrate, yielding nitrite as the sole free nitrogenous product. UV−visible stopped-flow and rapid-freeze-quench electron paramagnetic resonance data, along with product analysis, showed that the equilibrium between hydroxylamine and nitrite is fairly rapidly established in the presence of high initial concentrations of hydroxylamine, despite said equilibrium lying far to the left. By contrast, reduction of hydroxylamine to ammonia did not occur, even though disproportionation of hydroxylamine to yield both nitrite and ammonia is strongly thermodynamically favored. This suggests a kinetic barrier to the ccNiR-catalyzed reduction of hydroxylamine to ammonia. A mechanism for hydroxylamine reduction is proposed in which the hydroxide group is first protonated and released as water, leaving what is formally an NH_2^+ moiety bound at the heme active site. This species could be a metastable intermediate or a transition state but in either case would exist only if it were stabilized by the donation of electrons from the ccNiR heme pool into the empty nitrogen p orbital. In this scenario, ccNiR does not catalyze disproportionation because the electron-donating hydroxylamine does not poise the enzyme at a sufficiently low potential to stabilize the putative dehydrated hydroxylamine; presumably, a stronger reductant is required for this.

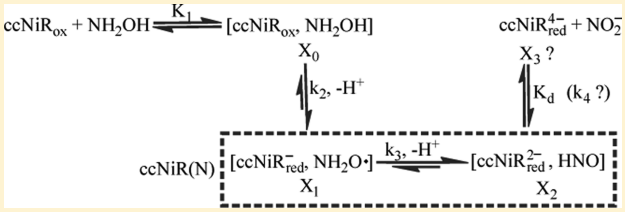

Microorganisms can extract energy from the environment by interconverting nitrite and ammonia in either direction. Under aerobic conditions, energy is extracted by ammonia-oxidizing bacteria (AOB) from the oxidation of ammonia by oxygen, whereas under anaerobic conditions, the energy is obtained by nitrite ammonifiers from the reduction of nitrite by organic electron donors.[1−3] Given that the thermodynamics of ammonia−nitrite interconversion can be readily shifted to favor one direction or the other simply by switching from aerobic to anaerobic conditions, the Pacheco research group is very interested in understanding how the individual enzymes that interconvert ammonia and nitrite are optimized to operate preferentially in one specific direction. During ammonification, the primary enzyme used is cytochrome *c* nitrite reductase (ccNiR, also termed nrfA), whereas the AOB use ammonia monooxygenase and hydroxylamine oxidoreductase (HAO) together to oxidize ammonia to nitrite. ccNiR and HAO share many gross structural similarities, invoking the question of whether they have been evolutionarily optimized to catalyze similar reactions in opposite directions. Previously, our group reported that HAO can be run in reverse by applying a sufficiently negative electrochemical potential to solutions of HAO and nitrite, nitric oxide, or hydroxylamine.[4,5] This work examines the extent to which ccNiR from the bacterium *Shewanella oneidensis* is capable of oxidizing hydroxylamine in the presence of high hydroxylamine concentrations.

ccNiR is a soluble protein located in the periplasm of several bacterial species, including *S. oneidensis*. This enzyme is a homodimer, with protomeric molecular masses ranging from 52 to 65 kDa (depending on the organism from which it is expressed), in which each protomer contains five *c*-type hemes.[6−11] Four of these hemes are six-coordinate, bis-histidine ligated, and low-spin. This motif is fairly ubiquitous in *c*-hemes used exclusively for electron transport, and indeed, the four hemes appear to act as shuttles that carry electrons from ccNiR's physiological electron donors to the active site.[7,12,13] The heme arrangement in ccNiR is such that they are closely packed, with iron−iron distances of <13 Å, which facilitates rapid inter-heme electron transfer.[14] The fifth *c*-type heme in ccNiR acts as the active site in each protomer. It is five-coordinate, allowing the substrate nitrite to bind to the open

Received: December 23, 2013
Revised: March 18, 2014
Published: March 19, 2014

dx.doi.org/10.1021/bi401705d | *Biochemistry* 2014, 53, 2136−2144

distal position, and is unique among *c*-hemes in that the axial ligand is a lysine residue. In addition to the five iron atoms from the hemes, each ccNiR protomer contains one buried six-coordinate Ca^{2+} ion per monomer in all ccNiRs characterized to date. In the case of *Desulfovibrio desulfuricans* ccNiR, the crystal structure shows a second six-coordinate Ca^{2+} ion in each monomer.[10]

The physiological electron donor for ccNiR depends on the organism from which it is derived. For *S. oneidensis*, the donor has been shown to be cymA, an inner-membrane electron transport protein.[13] In *Escherichia coli*, another γ-proteobacterium, the physiological donor has been identified as the soluble, periplasmic tetraheme protein nrfB, whereas other organisms, such as the δ-proteobacterium *D. desulfuricans* and the ε-proteobacterium *Wolinella succinogenes*, use an inner membrane protein known as nrfH as the electron donor to ccNiR.[7,12]

Physiologically, ccNiR performs the direct six-electron reduction of nitrite to ammonia with no unbound intermediates produced during catalysis. *In vitro*, the enzyme has also been shown to catalyze the five-electron reduction of nitric oxide, and the two-electron reduction of hydroxylamine, using the strong reductant methyl viologen monocation radical as an electron donor; in both cases, ammonia is the product.[15,16] Hydroxylamine is an interesting substrate because it can act as both an electron donor and an electron acceptor, which suggests that ccNiR could catalyze the reduction of hydroxylamine to ammonia using hydroxylamine itself as an electron donor. Such a reaction, known as disproportionation, is thermodynamically very favorable at pH 7 but was found not to occur in the presence of the potential catalyst HAO.[5] This study shows that ccNiR does not catalyze hydroxylamine disproportionation and explores the possible reasons.

MATERIALS AND METHODS

Protein Purification and Handling. *S. oneidensis* ccNiR was purified from a high-yield expression system as described previously by Youngblut et al.[17] Protein stocks were snap-frozen with liquid nitrogen and stored in aliquots at −80 °C until they were needed.

Stopped Flow. Stopped-flow experiments were conducted on a SF-61 DX2 Double Mixing Stopped-Flow System (Hi-Tech Scientific) that was made anaerobic by being scrubbed overnight with glucose oxidase (MP Biomedicals) and glucose (Fisher Scientific) at concentrations of 16 units/mL and 20 mM, respectively. Enzyme samples were made anaerobic in a tonometer by repeated cycles of gently applied vacuum followed by an argon purge with periodic agitation. All other solutions were made anaerobic by sparging syringes with argon for 10 min prior to mounting them on the instrument. All data were collected at 20 °C.

To prevent drastic pH changes when ccNiR was being mixed with high concentrations of hydroxylamine hydrochloride (Acros) during stopped-flow experiments, a double-mixing strategy was employed. Solutions of hydroxylamine hydrochloride were first rapidly mixed with 2-[4-(2-hydroxyethyl)-piperazin-1-yl]ethanesulfonic acid (HEPES) sodium salt (Fisher Scientific) at a hydroxylamine:HEPES ratio of 1:1.18 and aged for 1 s to reach a final pH of 7.0. This buffered hydroxylamine solution was then rapidly mixed with a 1.6 μM ccNiR solution in 20 mM HEPES and 1 mM ethylenediaminetetraacetic acid (pH 7.0). Spectral data were collected using a photodiode array detector (Hi-Tech Scientific) on both short (1.5 s) and long (30 s) time scales, after which the data sets were combined and analyzed using programs written within the commercially available software packages Mathcad 13.0 (PTC Software) and Origin 6.0 (Microcal Software). The analysis strategies used in our laboratory have been previously described;[4,5,17−19] details specific to this work are provided in the Results and as Supporting Information (sections S1−S3).

Rapid-Freeze-Quench EPR (RFQ-EPR). Rapid-freeze-quench samples were made using a model 715 syringe-ram controller (Update Instrument, Inc.) and quenched in −95 °C isopentane. The solutions were made anaerobic in a tonometer as described above and then withdrawn into a scrubbed gastight syringe for quenching, using an arrangement that preserved the anaerobicity by passing the solution from the tonometer through the stopped-flow syringes, and back out to the quench syringe. The quench syringes were those supplied with Update quench instruments. Reaction mixtures consisted of a final concentration of 200 mM hydroxylamine, 236 mM HEPES sodium salt, and 50 μM ccNiR (pH 7.0). EPR spectra were recorded at the Medical College of Wisconsin with 100 kHz magnetic-field modulation on an EleXsys E600 spectrometer (Bruker), equipped with an Oxford Instruments ITC503 temperature controller and an ESR900 helium flow cryostat (Oxford Instruments). Perpendicular mode EPR spectra were recorded at 9.39 GHz using an ER 4122SHQ resonator. Parallel mode data were recorded at the same frequency with the ER 4116DM instrument operating in TE012 mode. Precise frequencies were recorded for each spectrum by a built-in microwave counter. Background signals were recorded on a frozen water sample and subtracted in Xepr (Bruker Biospin) with small field corrections for slight frequency differences. Spectra were recorded at a temperature of 10 K and a microwave power of 5 mW. Other recording parameters were chosen such that the resolution was limited by the 10 G sinusoidal-field modulation amplitude. It was noted that a copper contaminant was present in several samples, so a mixture of hydroxylamine and HEPES sodium salt, as prepared previously, was rapidly mixed with 1 mM $CuSO_4$ in 20 mM HEPES (pH 7.0) using the same freeze-quench technique as previously described. This sample generated an EPR spectrum that was suitable for subtracting the copper contaminant from the previously generated data. Finally, intensities were normalized to the signal at 2290 G.

Nitrite/Nitric Oxide/Ammonia Assays. Two well-documented nitrite detection assays were used: the Griess assay[20] and the DAN assay.[21] Samples were prepared in an anaerobic glovebox with a 200 mM hydroxylamine solution and varying amounts of ccNiR. After 15 min, the ccNiR was removed using 10K molecular weight cutoff centrifugal concentrators (Millipore). To prevent hydroxylamine from possibly interfering with the assay, a 10% excess of sodium pyruvate was added to each reaction mixture, after which the assay was performed. Data were collected using a Varioskan Flash microtiter plate reader (Thermo Scientific).

Nitric oxide was assayed as described previously,[22] by conducting the same reaction as described above in the presence of 5 μM catalase (Sigma). Catalase binds nitric oxide tightly, leading to a characteristic change in the UV−vis spectrum that is readily quantified.

Ammonia was quantified using an established enzymatic assay[22] that had to be modified to first eliminate the interfering high-ionic strength solution that accompanied the high hydroxylamine concentrations. A reaction was first performed

dx.doi.org/10.1021/bi401705d | *Biochemistry* 2014, 53, 2136−2144

as described above for the nitrite detection assays. Once the enzyme had been removed by ultrafiltration, and the hydroxylamine by reaction with pyruvate, the solution pH was adjusted to 11.0. At this pH, ammonia in solution is gaseous; thus, the ammonia gas was selectively extracted across a Teflon membrane and into a pH 7, low-ionic strength (20 mM HEPES) solution, using apparatus described in the Supporting Information (section S4). This solution was subsequently assayed for ammonia concentration.

RESULTS

Stopped Flow. Figure 1 shows selected spectral changes observed after mixing 0.80 μM fully oxidized ccNiR (ccNiR$_{ox}$)

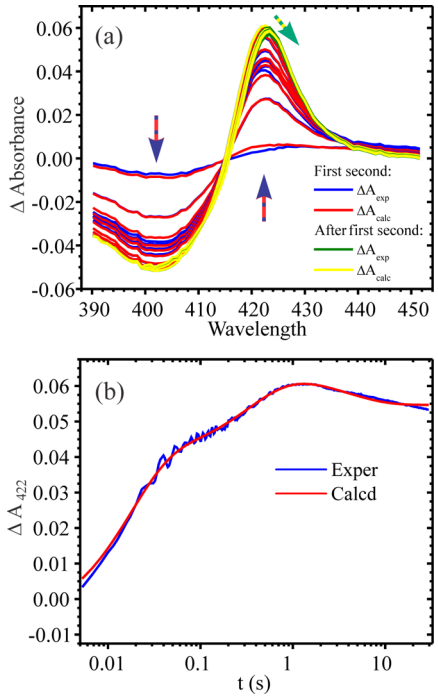

Figure 1. (a) UV−vis spectral changes observed at selected times after mixing 160 mM hydroxylamine with 0.80 μM ccNiR$_{ox}$, showing both experimental data and spectra calculated by least-squares fitting of the data with a three-exponential function, and four spectral components, X_0−X_3, as shown in Scheme 1. A decrease in the magnitude of the signal at ∼402 nm and an increase in the magnitude of the signal at ∼424 nm together indicate heme reduction. (b) Least-squares best fit of the ΔA vs t data at 422 nm.

Scheme 1. Minimal Kinetic Model for the Interaction of Hydroxylamine with ccNiR$_{ox}$

$$NH_2OH + ccNiR_{ox} \underset{}{\overset{K_1}{\rightleftharpoons}} X_0$$

$$X_0 \xrightarrow{k_2} X_1$$

$$X_1 \xrightarrow{k_3} X_2$$

$$X_2 \xrightarrow{k_4} X_3$$

with 160 mM hydroxylamine using the double-mixing stopped-flow method described above. The changes are broadly characteristic of low-spin c-heme reduction, exhibiting a maximal positive absorbance deflection at ∼422 nm, and a maximal negative amplitude at ∼402 nm.[23,24] Nevertheless, there are subtle shifts in the difference spectra over time (Figure 1a), and inspection of the time domain (Figure 1b) reveals that spectral changes occur on three distinct time scales: a fast phase that is complete within ∼100 ms, followed by two slower phases evolving over ∼1 and 30 s. Singular-value decomposition (SVD) analysis[25,26] revealed four spectral components. Subsequently, the SVD-processed spectra were fit to a model in which the first spectral component, X_0, was generated within the dead time of the stopped-flow instrument, after which X_0 was converted to species X_1−X_3 in three sequential steps, each governed by first-order kinetics (Scheme 1). The least-squares calculated spectra at selected times after mixing are overlaid on the experimental spectra in Figure 1a (red and yellow traces), while Figure 1b shows a fit of the trace collected at 422 nm. Figure 2a shows the extinction coefficient

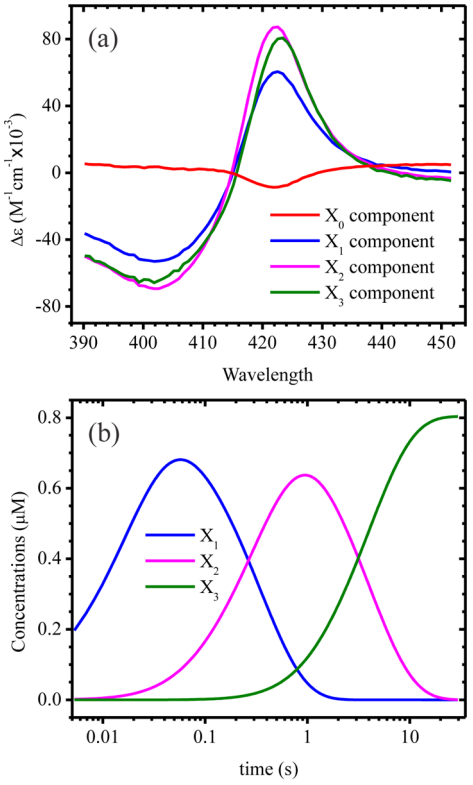

Figure 2. (a) Extinction coefficient difference spectra of spectral components X_0−X_3 (Scheme 1), calculated by fitting the data depicted in Figure 1 with a three-exponential function and four spectral components. The λ_{max} of the reduced heme peak at 424 nm increases in amplitude from the first intermediate to the second and then slightly decreases in amplitude and red-shifts going from the second intermediate to the final species. (b) Concentration vs time traces for species X_1−X_3, calculated by fitting the data depicted in Figure 1 as described above.

difference spectra calculated for each of the components in the Figure 1 fit, while Figure 2b shows how the concentration of each species is predicted to evolve over time.

When the experiment shown in Figures 1 and 2 was repeated using varying concentrations of hydroxylamine, the apparent rate constant for formation of component X_1 was found to vary hyperbolically with hydroxylamine concentration (Figure 3a). The apparent rate constant for formation of X_2 (k_{3obs}) appeared to increase slightly with hydroxylamine concentration [by at

dx.doi.org/10.1021/bi401705d | Biochemistry 2014, 53, 2136−2144

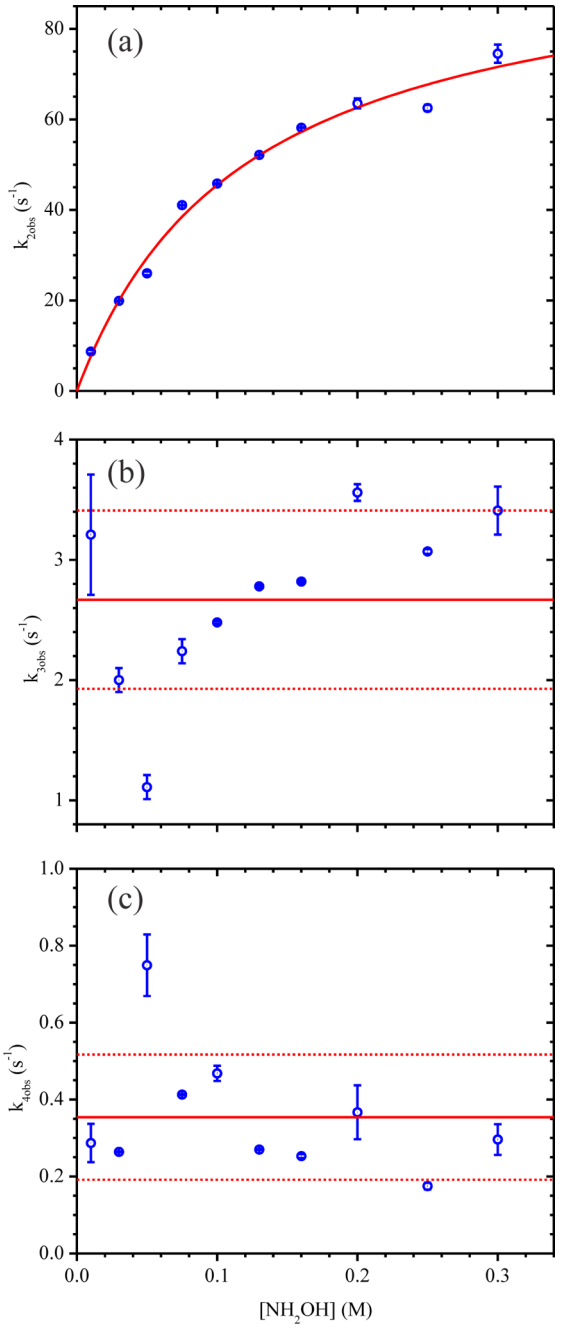

Figure 3. Dependence of the three apparent kinetic rate constants, (a) k_{2obs}, (b) k_{3obs}, and (c) k_{4obs}, obtained by fitting the ccNiR$_{ox}$–hydroxylamine UV–vis stopped flow data with three-exponential functions and four spectral components, on hydroxylamine concentration.

most a factor of 2 over the range from 0 to 300 mM hydroxylamine (Figure 3b)], while the apparent rate constant for formation of X_3 (k_{4obs}) was found to be essentially independent of hydroxylamine concentration (Figure 3c). These observations were interpreted in terms of the chemical model shown in Scheme 1, which for the moment ignores the possible slight dependence of k_{3obs} on hydroxylamine concentration. In this model, the fully oxidized ccNiR and added hydroxylamine first come to a rapid pre-equilibrium governed by equilibrium constant K_1. This pre-equilibrium is established within the dead time of the stopped-flow instrumentation and gives rise to the t_0 extinction coefficient difference spectrum (Figure 2a, X_0). The putative ccNiR–(NH_2OH) adduct then undergoes three sequential changes governed by rate constants k_2–k_4. A complete rate law derivation based in Scheme 1 is provided as Supporting Information (section S1).

The true second-order rate constant (k_2) for the first exponential event, together with the equilibrium constant (K_1), was obtained by fitting the data depicted in Figure 3a to a rectangular hyperbola (eq 1).

$$k_{2obs} = \frac{k_2[NH_2OH]}{K_1^{-1} + [NH_2OH]} \quad (1)$$

From this, k_2 and K_1^{-1} were determined to be 100 ± 6 s^{-1} and 120 ± 20 mM, respectively. Single values of k_3 and k_4, as would befit the Scheme 1 mechanism, were determined to be 2.7 ± 0.8 and 0.4 ± 0.2 s^{-1}, respectively, by averaging the values shown in panels b and c of Figure 3. The possibility that k_{3obs} actually is somewhat dependent on hydroxylamine concentration is considered further in the Discussion.

Rapid-Freeze-Quench EPR. The top three spectra in Figure 4 compare the perpendicular mode EPR spectra of

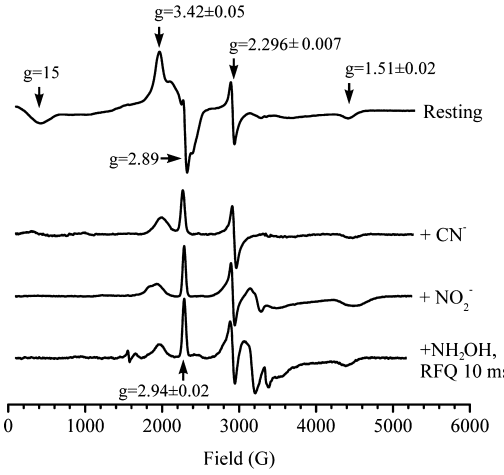

Figure 4. Variations in the X-band EPR spectrum of oxidized ccNiR as a function of solution properties: ccNiR in the absence of strong-field ligands, ccNiR with 200 mM cyanide, ccNiR with 200 mM nitrite, and ccNiR with 200 mM hydroxylamine (from top to bottom, respectively), freeze-quenched 10 ms after rapid mixing. Stopped-flow UV–vis data show that little ccNiR reduction takes place within 10 ms in solutions containing 200 mM hydroxylamine.

S. oneidensis ccNiR$_{ox}$ in the presence and absence of the strong-field ligands cyanide and nitrite. In the absence of strong-field ligands, one sees two characteristic g = 2.89 and 15 features (top trace, Figure 4), which are no longer present in the spectra obtained for the enzyme in the presence of cyanide and nitrite (middle two traces in Figure 4). The g = 15 feature is also visible in parallel mode (Supporting Information, section S5), whereas the other feature is not. On the basis of these results, the two features are assigned to the high-spin ($S = {}^5/_2$) Fe(III) active site, weakly exchange-coupled to one of the low-spin ($S = {}^1/_2$) hemes. The two features are similar to those assigned previously to the active site of *E. coli* ccNiR;[9] they are not present in the bottom two spectra of Figure 4 because the strong-field ligand cyanide or nitrite present in the samples

dx.doi.org/10.1021/bi401705d | *Biochemistry* 2014, 53, 2136–2144

binds to the active site, effecting a high-spin to low-spin transition.

Figure 5 shows the EPR spectra obtained for samples in which 50 μM ccNiR$_{ox}$ was mixed with 200 mM hydroxylamine

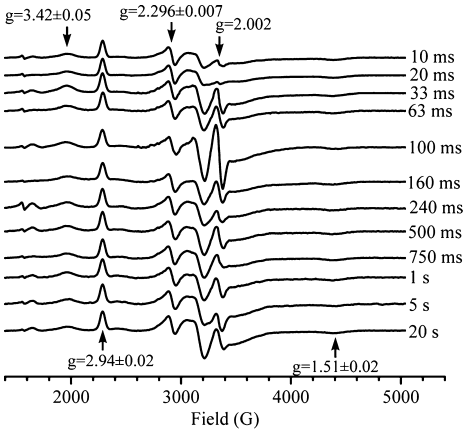

Figure 5. Results of the rapid-freeze-quench experiments. Changes observed in the X-band EPR spectrum of ccNiR at various times after rapid mixing of 50 μM resting enzyme with 200 mM hydroxylamine. All data were collected in perpendicular mode, at 9.39 GHz. Signals were normalized to the peak at 2290 G.

and then snap-frozen in cold isopentane at varying times after mixing, using the rapid-freeze-quench technique described in Materials and Methods. The spectrum for the first time point at 10 ms, also plotted as the bottom trace in Figure 4, is quite similar to that of ccNiR$_{ox}$ in the presence of the strong-field ligands cyanide and nitrite; in particular, the high-spin heme features assigned to the active site are no longer detectable. This is consistent with the establishment of a rapid pre-equilibrium in which hydroxylamine binds ccNiR$_{ox}$, as proposed on the basis of the stopped-flow results, and shown in the first step of Scheme 1. Presumably, binding of hydroxylamine to the active site heme results in a high-spin to low-spin transition in the same way that binding of cyanide or nitrite does.

The features present in the bottom three spectra of Figure 4 can all be assigned to low-spin Fe(III) hemes in a variety of environments. Three features (g_x = 2.94 ± 0.02, g_y = 2.296 ± 0.007, and g_z = 1.51 ± 0.02) can be attributed to low-spin hemes with imidazoles that are parallel to each other on opposite sides of the heme plane;[9,27] the *S. oneidensis* ccNiR crystal structure reveals two hemes with this imidazole arrangement.[17] The g = 3.42 ± 0.05 feature in all four of the spectra in Figure 4 is likely of a type termed a "highly anisotropic low-spin" (HALS) signal. This type of feature has been attributed to low-spin hemes with imidazoles perpendicular to each other on opposite sides of the heme plane.[9,27] Once again, the crystal structure of *S. oneidensis* ccNiR shows two hemes with this imidazole arrangement.[17] Note that the g_y and g_z features corresponding to the parallel imidazole hemes are also visible in the top spectrum of Figure 4, but the g_x feature is hidden by the active site high-spin heme features.

After the first 10 ms, there are surprisingly few changes in the EPR spectrum of the NH_2OH–ccNiR reaction mixture, with the important exception of a g = 2.002 signal with an intensity that reaches its maximum within 100 ms and then decreases to a background value of ~20% (Figure 5). This signal is clearly attributable to a free radical species. For the reaction conditions given, the first stopped-flow kinetic intermediate (see above) is expected to reach a maximal concentration after ~50 ms and the second after ~1 s. Thus, the radical species signal intensity reaches a maximum on roughly the same time scale as the first stopped-flow kinetic intermediate signal does. This suggests that the first kinetic process involves a one-electron transfer from the bound hydroxylamine moiety to the ccNiR heme pool, which generates a $NH_2O^\bullet$ radical seen by EPR, and the reduced heme signal seen by the UV–vis stopped-flow method. The second kinetic process would then involve the transfer of an electron from $NH_2O^\bullet$ to the ccNiR heme pool. This would explain the loss of the free radical signal in the EPR spectrum after the first 100 ms (Figure 5) and the subsequent increase in absorption at 422 nm attributed to heme reduction, which reaches a maximum after ~1 s (Figures 1 and 2). The fact that the EPR free radical signal does not vanish completely after 100 ms suggests that the processes governed by k_3 and k_4 (Scheme 1) actually result in the establishment of equilibria among species X_1–X_3, rather than in complete conversion to X_3. Note, however, that the apparent extinction coefficient difference spectra calculated for X_1–X_3 in the stopped-flow experiments show little dependence on hydroxylamine concentration beyond ~20 mM NH_2OH (Supporting Information, section S2), indicating that under these conditions only small amounts of ccNiR remain completely unreduced as equilibrium is approached. By contrast, at hydroxylamine concentrations below ~20 mM, stopped-flow experiments show that the extent of ccNiR reduction at equilibrium decreases with a decreasing hydroxylamine concentration (Supporting Information, section S2).

Assays for Free Reactive Nitrogen Species. Solutions containing 200 mM hydroxylamine and concentrations of ccNiR varying from 1 to 90 μM were allowed to react anaerobically for ~15 min and then analyzed for the presence of free nitric oxide, nitrite, and ammonium, as described in Materials and Methods. Of the three nitrogenous species, only nitrite was detected; Figure 6 shows the observed dependence

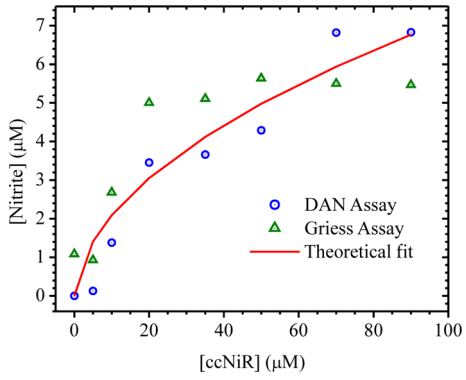

Figure 6. Results of the nitrite detection assays. Both the colorimetric Griess assay (green triangles, ref 20) and the fluorometric DAN assay (blue circles, ref 21) were used. The red trace is the least-squares best fit to eq 2.

of free nitrite concentration generated on the total ccNiR concentration. At all ccNiR concentrations, the concentration of free nitrite generated is lower than the total ccNiR concentration, and the $[NO_2^-]_{free}/[ccNiR]_{total}$ ratio decreases with an increase in $[ccNiR]_{total}$. This behavior is consistent with the establishment of the net equilibrium shown in Scheme 2. The initial reaction of hydroxylamine with ccNiR leads to the formation of a mixture of species collectively termed ccNiR(N),

dx.doi.org/10.1021/bi401705d | *Biochemistry* 2014, 53, 2136–2144

Scheme 2. Minimal Thermodynamic Model for the Interaction of Hydroxylamine with ccNiR$_{ox}$

$$ccNiR_{ox} + NH_2OH \rightleftharpoons ccNiR(N)$$

$$ccNiR(N) \overset{K_d}{\rightleftharpoons} ccNiR^{4-} + NO_2^-$$

in which nitrogen-containing moieties are bound to the active site, and the heme pool is reduced by varying degrees. In turn, the species represented by ccNiR(N) are in equilibrium with free nitrite and ccNiR species in which the heme pool is reduced by four electrons. On the basis of Scheme 2, one can derive eq 2

$$[NO_2^-]_{free} = -0.5K_d + 0.5\sqrt{K_d^2 + 4K_d[ccNiR]_t} \quad (2)$$

which gives the concentration of free nitrite as a function of the total ccNiR concentration (Supporting Information, section S3). The data depicted in Figure 6 were fit to eq 2 (red trace in Figure 6), which yielded a K_d value of 0.4 μM for dissociation of free nitrite from ccNiR(N).

DISCUSSION

Scheme 3 presents a minimal mechanism for the reaction of ccNiR with hydroxylamine, which combines the simple kinetic model of Scheme 1 with the equilibrium model of Scheme 2, taking into account the consolidated stopped-flow and RFQ-EPR results, together with those of the assays for free reactive nitrogen species. The assignments for kinetic species X_0 and X_1 are strongly supported by both the stopped-flow and RFQ-EPR data. In the first spectrum of the RFQ-EPR series (collected at 10 ms), no signal attributable to high-spin heme is detected, indicating that hydroxylamine has bound to ccNiR and induced a high-spin to low-spin transition (Figure 4, bottom trace, and Figure 5, top trace). At this same point in the reaction, the stopped-flow data show that minimal reduction of ccNiR has yet occurred. Therefore, within the dead time of both the stopped-flow and RFQ instrumentation, hydroxylamine has bound to the active site of ccNiR and induced a transition from high-spin heme to low-spin heme, but little electron transfer from bound hydroxylamine to the heme pool has occurred. The presence of the pre-equilibrium is further supported by the apparent dependence of rate constant k_{2obs}, which governs conversion of X_0 to X_1, on hydroxylamine concentration (Figure 3a).

Scheme 3. Minimal Model for the Interaction of Hydroxylamine with ccNiR$_{ox}$ That Considers Kinetic and Thermodynamic Observations[a]

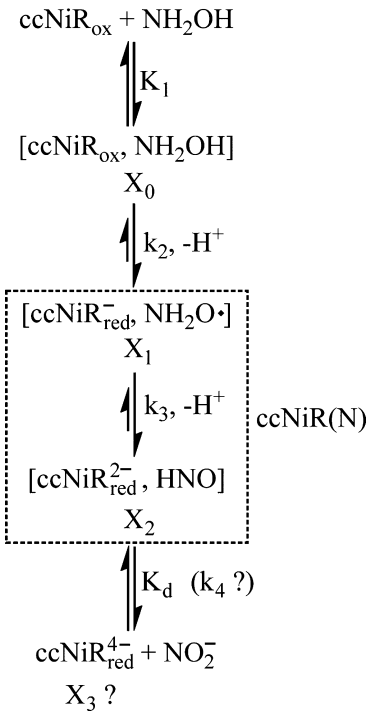

[a]The assignments of X_0 and X_1 are well supported by the data and those of X_2 and X_3 less so (see Discussion).

Conversion of kinetic species X_0 to X_1 is assigned as an intramolecular one-electron transfer from the bound hydroxylamine to the heme pool. In the stopped-flow experiments with 200 mM hydroxylamine, the ccNiR$_{red}^-$ signal reaches a maximum at ~50 ms, which correlates reasonably well with the RFQ-EPR 100 ms time point at which the g = 2.002 free radical feature reaches its maximal intensity (Figure 5). Given the known chemistry of hydroxylamine, the unpaired electron is most likely on the oxygen atom of the substrate molecule,[28] although experiments with ^{15}N-labeled hydroxylamine would have to be conducted to explicitly confirm this.

The relative insensitivity to hydroxylamine concentration, at >20 mM NH_2OH, of the extinction coefficient difference spectra for species X_1–X_3 (Supporting Information, section S2), shows that virtually all ccNiR is eventually reduced by at least one electron under these conditions. Beyond this observation though, the assignments made in Scheme 3 for kinetic species X_2, and even more so for X_3, are substantially less certain than those made for X_0 and X_1. From 100 ms to ~1 s, the UV–vis spectral changes associated with the appearance of kinetic species X_2 are consistent with further reduction of the ccNiR heme pool (Figures 1 and 2). During the same time period, the RFQ-EPR data show that the intensity of the free radical feature decreases but does not disappear completely; no other changes in the EPR spectra can be readily detected (Figure 5). The minimal model of Scheme 3 attributes the reduction event governed by rate constant k_3, resulting in the formation of kinetic species X_2, to a second one-electron intramolecular electron transfer, which leaves the heme pool reduced by two electrons and a HNO moiety bound at the active site. The incomplete disappearance of the X_1 free radical signal during this time interval, however, shows that the process governed by k_3 is actually an approach to equilibrium between kinetic species X_1 and X_2. Thus, one is actually measuring $k_{3obs} = k_3 + k_{-3}$ in the stopped-flow experiments. Similarly, in the absence of EPR spectral changes that can be definitively attributed to chemical changes in the heme pool during the interval governed by k_{3obs}, one cannot rule out the possibility that X_2 represents not just one reduced ccNiR species but several, all in rapid equilibrium with each other relative to the rate constant for their formation, k_{3obs}.

Beyond 1 s, the appearance of kinetic species X_3 results in a slight red shift of the associated extinction coefficient spectrum, but little change in amplitude at 422 nm (Figure 1). At present, there is insufficient information to assign this kinetic event with any certainty. It is possible that k_{4obs} is directly associated with the K_d obtained from the free nitrite assays, in which case X_3 would be attributed to the four-electron-reduced ccNiR moiety generated by nitrite release, as suggested in Scheme 3.

dx.doi.org/10.1021/bi401705d | Biochemistry 2014, 53, 2136–2144

However, many other interpretations of these data are equally plausible.

A notable limitation of the model of Scheme 3 is that it completely neglects the dimeric nature of ccNiR and instead treats the subunits as uncoupled monomers. This is a crude approximation given that recent protein film voltammetry studies provide evidence of cooperativity between the protomers.[29] The data presented herein do not justify the use of a model more elaborate than Scheme 3 for their interpretation, but future studies for testing for the evidence of cooperativity are planned. A less constricting limitation of Scheme 3 is that it provides no way of accounting for the possible slight dependence of k_{3obs} on hydroxylamine concentration (Figure 3b). The apparent dependence may well be an artifact of the fitting procedure, whereby the strong dependence of k_{2obs} is slightly admixed into an independent k_{3obs}. One possible explanation for a true dependence of k_{3obs} on hydroxylamine concentration would be if this rate constant governed nitrite dissociation, and if the dissociation step were dependent on substitution of nitrite with hydroxylamine at the active site. Again, many other explanations are equally plausible, and embellishments of the model of Scheme 3 will have to await more detailed studies.

A very important result of this work is the revelation that $ccNiR_{ox}$ is incapable of catalyzing the disproportionation of hydroxylamine (Scheme 4). If this process were possible, then

Scheme 4. Thermodynamics of Hydroxylamine Disproportionation at pH 7

$$2NH_2OH + 6H^+ + 4e^- \longrightarrow 2NH_4^+ + H_2O \qquad \varepsilon^o_1 = 0.89V$$

$$NH_2OH + H_2O \longrightarrow NO_2^- + 5H^+ + 4e^- \qquad -\varepsilon^o_2 = -0.27V$$

$$3NH_2OH + H^+ \longrightarrow 2NH_4^+ + NO_2^- + H_2O \qquad \varepsilon^o_{disp} = 0.62V$$

under the reaction conditions of Figure 6, in which 200 mM hydroxylamine and no disproportionation products were present at the outset, large quantities of both ammonium and nitrite would have been generated. Instead, only substoichiometric amounts of nitrite were detected. Hydroxylamine disproportionation is highly thermodynamically favorable [ε° = 0.62 V (Scheme 4)], so the barrier to the process must be a kinetic one. At first glance though, ccNiR seems to be ideally suited for catalyzing hydroxylamine disproportionation, which is illustrated schematically in Figure 7. Crystal structures of ccNiR reveal what appears to be a "molecular wire" composed of six-coordinate *c*-hemes that effectively connects the two active sites within the homodimer.[6−11,17] Thus, as suggested in Figure 7, electrons released by hydroxylamine oxidation at the active site of one protomer should be readily transferred within the enzyme to drive hydroxylamine reduction at the active site of the other protomer. Such intersubunit electron transfer might be prevented by some factor not revealed in the crystal structure, but this seems unlikely in light of recent protein film voltammetry studies that show the protomers acting cooperatively.[29] Our results show that ccNiR does stoichiometrically oxidize hydroxylamine to nitrite on the time scale of seconds, although the equilibrium for free nitrite release lies far to the left (K_d = 0.4 μM from analysis of the data depicted in Figure 6). This leaves the thermodynamically very favorable reduction of hydroxylamine to ammonium as the most likely kinetic barrier to disproportionation.

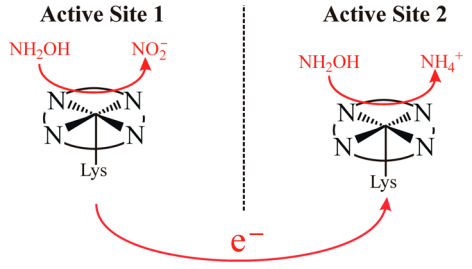

Figure 7. Putative mechanism by which ccNiR could catalyze hydroxylamine disproportionation (the process, however, is not observed). Hydroxylamine is oxidized to nitrite at the active site of one subunit of ccNiR, and the electrons produced in the reaction are transferred across the dimer interface (dashed line) to the active site of the other subunit, where hydroxylamine is reduced to ammonium. Note that this simplified figure does not reflect the stoichiometry of the disproportionation process, which is correctly given in Scheme 4: oxidation of 1 equiv of hydroxylamine to nitrite yields enough electrons to reduce 2 equiv of hydroxylamine to ammonium.

Figure 8 outlines one possible mechanism for the reduction of hydroxylamine to ammonium at the ccNiR active site that would explain why disproportionation is not catalyzed by this enzyme. In Figure 8, the hydroxide moiety of the bound hydroxylamine is first protonated and released as water. This results in the formation of the species notionally represented by resonance structures "B". Such a species would be stable only when the ccNiR heme pool is collectively poised at a sufficiently low potential to effectively make B an amide bound to Fe^{III} (right resonance form). According to this mechanism, hydroxylamine disproportionation does not occur because the oxidative half-reaction does not poise the hemes at sufficiently low potentials to stabilize intermediate B. Figure 8 portrays hydroxylamine reduction as occurring via a concerted two-electron process that generates the amide, but a similar explanation for the lack of ccNiR-catalyzed disproportionation can be readily formulated on the basis of a mechanism in which hydroxylamine reduction takes place via sequential one-electron transfers, as recently suggested by Judd et al.[29] The key insight of Figure 8 is that the heme pool must be poised at a potential below a certain threshold to permit the removal of hydroxide from hydroxylamine.

As mentioned in the introductory section, the enzyme HAO is also incapable of catalyzing disproportionation, despite possessing an architecture apparently ideal for fostering the process.[4,5] The midpoint potential of the HAO active site is substantially more negative than that of ccNiR (−260 mV versus NHE[30] compared to our as yet unpublished value of 20 mV versus NHE for the active site of ccNiR in the presence of a coordinated strong-field ligand). Thus, the rationale presented in Figure 8 would apply equally well to HAO, though additional factors could also contribute to thwarting disproportionation in this enzyme.[5] Disproportionation catalyzed by $[Fe(CN)_5H_2O]^{3-}$ [31] and by water-soluble iron(III) porphyrinate compounds[32] has been reported, but interestingly, in both cases, the oxidation products were N_2 and N_2O in proportions varying with specific reaction conditions. In neither case were detectable amounts of nitrite or other monomeric nitrogen oxidation products detected. An interesting open question is whether the active sites of ccNiR or HAO could be tuned by site-directed mutagenesis to catalyze disproportionation of hydroxylamine to yield both ammonia and monomeric nitrogen oxidation products.

dx.doi.org/10.1021/bi401705d | *Biochemistry* 2014, 53, 2136−2144

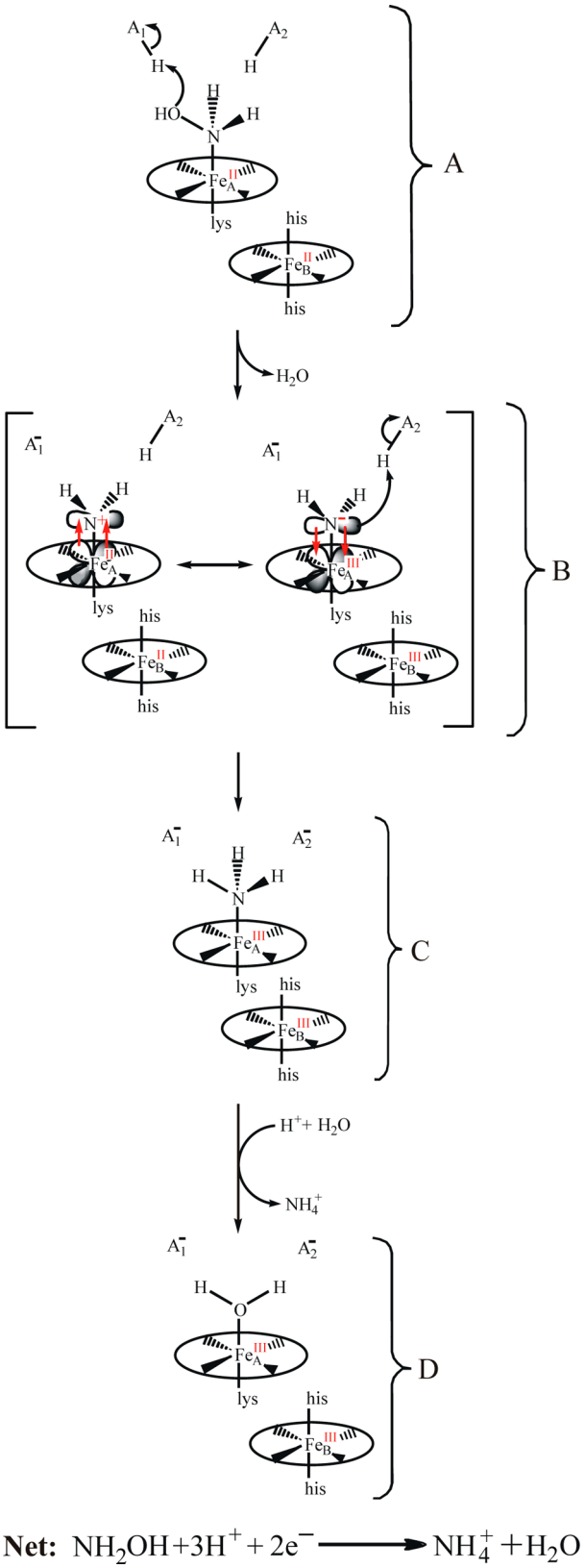

Net: $NH_2OH + 3H^+ + 2e^- \longrightarrow NH_4^+ + H_2O$

Figure 8. One possible mechanism for the reduction of hydroxylamine to ammonium at the ccNiR active site. For reduction to occur, the right resonance structure of species B must dominate.

To summarize, despite the manifestly nonphysiological nature of the $ccNiR_{ox}$ + NH_2OH reaction discussed herein, the results of this study provide important insights about the final step of the physiologically relevant ccNiR-catalyzed reduction of nitrite, namely reduction of heme-bound hydroxylamine to ammonium. In addition to the theoretical significance of these results, they are also proving to be very useful in the design of follow-up experiments. For example, the results show that though reduction of hydroxylamine to ammonium is unlikely to occur at applied potentials greater than approximately −100 mV versus NHE, interconversion of nitrogenous species with formal oxidation states between −1 (hydroxylamine level) and +3 (nitrite level) could very well occur at applied potentials between 0 and −100 mV versus NHE. So far, this insight has been used to prepare and characterize partially reduced ccNiR(N) species (as defined in Scheme 2), and studies of the reactivity of these species are now under way.

■ ASSOCIATED CONTENT

Ⓢ Supporting Information

Rate law derivation for the minimal Scheme 1 mechanism, amplitudes of the extinction coefficient difference spectra obtained in stopped-flow experiments for species X_1−X_3 (evidence of reversibility), the derivation of eq 2, an assay for ammonia in high-ionic strength solutions, and a parallel mode EPR spectrum of $cNiR_{ox}$. This material is available free of charge via the Internet at http://pubs.acs.org.

■ AUTHOR INFORMATION

Corresponding Author

*E-mail: apacheco@uwm.edu. Phone: (414) 229-4413. Fax: (414) 229-5530.

Present Addresses

∥M.Y.: Energy Biosciences Institute, University of California, 2151 Berkeley Way, Berkeley, CA 94704.

⊥D.W.: Department of Chemistry, University of California, One Shields Ave., Davis, CA 95616.

Funding

Supported by National Science Foundation Grant MCB-1121770.

Notes

The authors declare no competing financial interest.

■ ACKNOWLEDGMENTS

We are grateful to Professor Joseph Aldstadt for his help in designing an ionic strength-insensitive ammonia assay.

■ ABBREVIATIONS

AOB, ammonia-oxidizing bacteria; ccNiR, cytochrome *c* nitrite reductase; $ccNiR_{ox}$, resting (fully oxidized) ccNiR; HAO, hydroxylamine oxidoreductase; RFQ-EPR, rapid-freeze-quench electron paramagnetic resonance; HALS, highly anisotropic low-spin signal; SVD, singular-value decomposition.

■ REFERENCES

(1) Ehrlich, H. L. (2002) *Geomicrobiology*, 4th ed., Marcel Dekker, Inc., New York.

(2) Fenchel, T., King, G. M., and Blackburn, T. H. (1998) *Bacterial Biogeochemistry*, 2nd ed., Academic Press, London.

(3) Canfield, D. E., Glazer, A. N., and Falkowski, P. G. (2010) The Evolution and Future of Earth's Nitrogen Cycle. *Science 330*, 192−196.

(4) Kostera, J., Youngblut, M. D., Slosarczyk, J. M., and Pacheco, A. A. (2008) Kinetic and product distribution analysis of NO reductase activity in *Nitrosomonas europaea* hydroxylamine oxidoreductase. *J. Biol. Inorg. Chem. 13*, 1073−1083.

(5) Kostera, J., McGarry, J. M., and Pacheco, A. A. (2010) Enzymatic Interconversion of Ammonia and Nitrite: The Right Tool for the Job. *Biochemistry 49*, 8546−8553.
(6) Einsle, O., Messerschmidt, A., Stach, P., Bourenkov, G. P., Bartunik, H. D., Huber, R., and Kroneck, P. M. H. (1999) Structure of cytochrome c nitrite reductase. *Nature 400*, 476−480.
(7) Einsle, O., Stach, P., Messerschmidt, A., Simon, J., Kroger, A., Huber, R., and Kroneck, P. M. H. (2000) Cytochrome c nitrite reductase from *Wolinella succinogenes*: Structure at 1.6 angstrom resolution, inhibitor binding, and heme-packing motifs. *J. Biol. Chem. 275*, 39608−39616.
(8) Pereira, I., LeGall, J., Xavier, A., and Teixeira, M. (2000) Characterization of a heme *c* nitrite reductase from a non-ammonifying microorganism, *Desulfovibrio vulgaris* Hildenborough. *Biochim. Biophys. Acta 1481*, 119−130.
(9) Bamford, V. A., Angove, H. C., Seward, H. E., Thomson, A. J., Cole, J. A., Butt, J. N., Hemmings, A. M., and Richardson, D. J. (2002) Structure and spectroscopy of the periplasmic cytochrome c nitrite reductase from *Escherichia coli*. *Biochemistry 41*, 2921−2931.
(10) Cunha, C. A., Macieira, S., Dias, J. M., Almeida, G., Goncalves, L. L., Costa, C., Lampreia, J., Huber, R., Moura, J. J. G., Moura, I., and Romao, M. J. (2003) Cytochrome c nitrite reductase from *Desulfovibrio desulfuricans* ATCC 27774: The relevance of the two calcium sites in the structure of the catalytic subunit (NrfA). *J. Biol. Chem. 278*, 17455−17465.
(11) Rodrigues, M. L., Oliveira, T., Matias, P. M., Martins, C., Valente, F. M., Pereira, I. A., and Archer, M. (2006) Crystallization and preliminary structure determination of the membrane-bound complex cytochrome c nitrite reductase from *Desulfovibrio vulgaris* Hildenborough. *Acta Crystallogr. F62*, 565−568.
(12) Rodrigues, M., Oliveira, T., Pereira, I., and Archer, M. (2006) X-ray structure of the membrane-bound cytochrome *c* quinol dehydrogenase NrfH reveals novel haem coordination. *EMBO J. 25*, 5951−5960.
(13) Gao, H., Yang, Z. K., Barua, S., Reed, S. B., Romine, M. F., Nealson, K. H., Fredrickson, J. K., Tiedje, J. M., and Zhou, J. (2009) Reduction of nitrate in *Shewanella oneidensis* depends on atypical NAP and NRF systems with NapB as a preferred electron transport protein from CymA to NapA. *ISME J. 3*, 966−976.
(14) Burlat, B., Gwyer, J. D., Poock, S., Clarke, T., Cole, J. A., Hemmings, A. M., Cheesman, M. R., Butt, J. N., and Richardson, D. J. (2005) Cytochrome c nitrite reductase: From structural to physicochemical analysis. *Biochem. Soc. Trans. 33*, 137−140.
(15) Einsle, O., Messerschmidt, A., Huber, R., Kroneck, P. M. H., and Neese, F. (2002) Mechanism of the six-electron reduction of nitrite to ammonia by cytochrome c nitrite reductase. *J. Am. Chem. Soc. 124*, 11737−11745.
(16) Poock, S., Leach, E., Moir, J., Cole, J., and Richardson, D. (2002) Respiratory Detoxification of Nitric Oxide by the Cytochrome *c* Nitrite Reductase of *Escherichia coli*. *J. Biol. Chem. 277*, 23664−23669.
(17) Youngblut, M., Judd, E. T., Srajer, V., Sayyed, B., Goelzer, T., Elliott, S. J., Schmidt, M., and Pacheco, A. A. (2012) Laue crystal structure of *Shewanella oneidensis* cytochrome *c* nitrite reductase from a high-yield expression system. *J. Biol. Inorg. Chem. 17*, 647−662.
(18) Purwar, N., McGarry, J. M., Kostera, J., Pacheco, A. A., and Schmidt, M. (2011) Interaction of nitric oxide with catalase: Structural and kinetic analysis. *Biochemistry 50*, 4491−4503.
(19) Cabail, M. Z., Moua, V., Bae, E., Meyer, A., and Pacheco, A. A. (2007) Quantifying the photoinduced release of nitric oxide from N,N′-bis(carboxymethyl)-N,N′-dinitroso-1,4-phenylenediamine. Effect of reducing agents on the mechanism of the photoinduced reactions. *J. Phys. Chem. A 111*, 1207−1213.
(20) Griess, P. (1879) Ueber einige azoverbindungen. *Chem. Ber. 12*, 426−428.
(21) Nussler, A. K., Glanemann, M., Schirmeier, A., Liu, L., and Nussler, N. C. (2006) Fluorometric measurement of nitrite/nitrate by 2,3-diaminonaphthalene. *Nat. Protoc. 1*, 2223−2226.
(22) Pacheco, A. A., McGarry, J. M., Kostera, J., and Corona, A. (2011) Techniques for investigating hydroxylamine disproportionation by hydroxylamine oxidoreductases. *Methods Enzymol. 486*, 447−463.
(23) Gouterman, M. (1978) Optical Spectra and Electronic Structure of Porphyrins and Related Rings. In *The Porphyrins V3* (Dolphin, D., Ed.) pp 1−166, Academic Press, Inc., San Diego.
(24) Adar, F. (1978) Electronic Absorption Spectra of Hemes and Hemoproteins. In *The Porphyrins V3* (Dolphin, D., Ed.) pp 167−210, Academic Press, Inc., San Diego.
(25) Press, W. H., Teukolsky, S. A., Vetterling, W. T., and Flannery, B. P. (2007) *Numerical Recipes in C: The art of scientific computing*, 3rd ed., pp 65−75, Cambridge University Press, New York.
(26) Henry, E. R., and Hofrichter, J. (1992) Singular Value Decomposition: Application to Analysis of Experimental Data. In *Methods in Enzymology* (Brand, L., and Johnson, M. L., Eds.) pp 129−192, Academic Press, San Diego.
(27) Walker, F. A. (1999) Magnetic spectroscopic (EPR, ESEEM, Mossbauer, MCD and NMR) studies of low-spin ferriheme centers and their corresponding heme proteins. *Coord. Chem. Rev. 186*, 471−534.
(28) Wieghardt, K. (1984) in *Advances in Inorganic and Bioinorganic Mechanism* (Sykes, A. G., Ed.) Vol. 3, p 213, Academic Press, London.
(29) Judd, E. T., Youngblut, M., Pacheco, A. A., and Elliott, S. J. (2012) Direct Electrochemistry of *Shewanella oneidensis* Cytochrome c Nitrite Reductase: Evidence of Interactions across the Dimeric Interface. *Biochemistry 51*, 10175−10185.
(30) Collins, M. J., Arciero, D. M., and Hooper, A. B. (1993) Optical Spectropotentiometric Resolution of the Hemes of Hydroxylamine Oxidoreductase: Heme Quantitation and pH-Dependence of E_m. *J. Biol. Chem. 268*, 14655−14662.
(31) Alluisetti, G. E., Almaraz, A. E., Amorebieta, V. T., Doctorovich, F. A., and Olabe, J. A. (2004) Metal-catalyzed anaerobic disproportionation of hydroxylamine. Role of diazene and nitroxyl intermediates in the formation of N_2, N_2O, NO^+ and NH_3. *J. Am. Chem. Soc. 126*, 13432−13442.
(32) Bari, S. E., Amorebieta, V. T., Gutierrez, M. M., Olabe, J. A., and Doctorovich, F. A. (2010) Disproportionation of hydroxylamine by water-soluble iron(III) porphyrinate compounds. *J. Inorg. Biochem. 104*, 30−36.